Journal of Solid Mechanics Vol. 13, No. 1 (2021) pp. 37-53
DOI: 10.22034/jsm.2020.1884938.1524

Thermal Buckling Analysis of Porous Conical Shell on Elastic Foundation

M. Gheisari, M.M. Najafizadeh*, A.R. Nezamabadi, S. Jafari, P.Yousefi

Department of Mechanical Engineering, Islamic Azad University, Arak Branch, Arak, Iran

Received 3 September 2020; accepted 8 December 2020

ABSTRACT

In this research, the thermal buckling analysis of a truncated conical shell made of porous materials on elastic foundation is investigated. The equilibrium equations and the conical shell`s stability equations are obtained by using the Euler`s and the Trefftz equations .Properties of the materials used in the conical shell are considered as porous foam made of steel, which is characterized by its non-uniform distribution of porous materials along the thickness direction. Initially, the displacement field relation based on the classical model for double-curved shell is expressed in terms of the Donnell`s assumptions. Non-linear strain-displacement relations are obtained according to the von Kármán assumptions by applying the Green-Lagrange strain relationship. Then, performing the Euler equations leads obtaining nonlinear equilibrium equations of cylindrical shell. The stability equations of conical shell are obtained based on neighboring equilibrium benchmark (adjacent state). In order to solve the stability equations, primarily, due to the existence of axial symmetry, we consider the cone crust displacement as a sinusoidal geometry, and then, using the generalized differential quadrature method, we solve them to obtain the critical temperature values of the buckling Future. In order to validate the results, they compare with the results of other published articles. At the end of the experiment, various parameters such as dimensions, boundary conditions, cone angle, porosity parameter and elastic bed coefficients are investigated on the critical temperature of the buckling.

Keywords: Thermal buckling; Truncated conical shell; Porous materials; General differential quadrature; Elastic foundation.

1 INTRODUCTION

USING the improved Donnell equations in the thermal buckling analysis of thin cylindrical shells was perused by Eslami et al. [1]. Buckling of FGM cylindrical shells reinforced by rings and stringers under axial compression with the stability equations linearized in terms of displacements was investigated by Najafizadeh et al.

*Corresponding author. Tel.: +98 8634134025.
E-mail address: m-najafizadeh@iau-arak.ac.ir (M.M.Najafizadeh)

[2]. Considering the stiffeners and skins made of functionally graded materials that their properties vary continuously through the thickness direction, was observed in their study. Deliberating analysis of dynamic behavior of functionally graded conical shells, cylindrical shells and annular plates was accomplished by Tornabene et at. [3, 4]. In order to scrutinize the above moderately thick structural elements, the First-order Shear Deformation Theory (FSDT) was used. When surmising the materials to be isotropic and inhomogeneous through the direction of the thickness, the treatment was instigated within the theory of linear elasticity. The mechanical buckling of functionally graded cylindrical shell embedded in an outer elastic medium, and subjected to combined axial and radial compressive loads was investigated by Bagherizadeh et al. [5]. Based on a higher-order shear deformation theory, the theoretical formulations are presented by pondering the transverse shear strains. Applying the nonlinear strain–displacement relations of FGM cylindrical shells leads to obtaining the governing equations. For modelling the elastic foundation, a two-parameter Pasternak model obtained by adding a shear layer to the Winkler model is used. Bagherizadeh et al. [6] reviewed the thermal buckling of an FG cylindrical shell on a Pasternak-type elastic foundation. In this survey, the stability equations of the shell are decoupled to inaugurate an equation in terms of only the out of- plane displacement component. Sofiyev and Kuruoglu [7] perused the torsional vibration and buckling analysis of a cylindrical shell with functionally graded (FG) coatings surrounded by an elastic medium. The material properties of the FG coatings are assumed to be graded in the thickness direction according to a simple power law distribution in terms of the volume fractions of the constituents. A two-parameter foundation model or Pasternak foundation model is used to describe the shell–foundation interaction. Dung and Hoa [8–10], obtained the results on the static and dynamic nonlinear buckling and post buckling analysis of eccentrically stiffened FGM circular cylindrical shells under external pressure and torsional loads. The material properties of the shell and the stiffeners are assumed to be continuously graded in the thickness direction. The Galerkin method was used to obtain closed-form expressions to determine critical buckling loads. Sabzikar Boroujerdy et al. [11] presented buckling of a heated temperature dependent FGM cylindrical shell surrounded by an elastic medium based on the Donnell theory of shells combined with the von Karman type of geometrical nonlinearity. Equivalent properties of the shell are obtained based on the Voigt rule of mixture in terms of a power law volume fraction for the constituents. The properties of the constituents are considered temperature dependent. The temperature profile through the shell thickness is obtained by means of the central finite difference method. Linear pre-buckling analysis is performed to obtain the pre-buckling forces of the cylindrical shell. Stability equations are derived based on the well-known adjacent equilibrium criterion. Three coupled partial differential stability equations are solved with the aid of a hybrid Fourier-GDQ method. Thermal bifurcation behavior of cross-ply laminated composite cylindrical shells reinforced with shape memory alloy fibers is investigated by Asadi et al. [12]. The properties of the constituents are assumed to be temperature dependent. Donnell's kinematic assumptions accompanied by the von Karman type of geometrical nonlinearity are used to derive governing equations of the shell. Furthermore, the one-dimensional constitutive law of Brinson is used to predict the behavior of the shape memory alloy fibers through the heating process. The governing equilibrium equations are established by employing the static version of the virtual displacements principle. A linear thermal buckling analysis of truncated hybrid FGM conical shells based on the classical shell theory using Sanders nonlinear kinematics equations was analyzed by Torabi et al. [13]. Dung et al. [14] studied linear buckling of FGM thin truncated conical shells reinforced by homogeneous eccentric stringers and rings subjected to axial compressive load and uniform external pressure load based on the smeared stiffeners technique and the classical shell theory. Sofiyev and Kuruoglu [15] studied the nonlinear buckling behavior of FGM truncated conical shells surrounded by an elastic medium based on the classical shell theory and applying Galerkin method. Bahadori and Najafizadeh [16] derived the vibration characteristics of simply supported 2D-FG cylindrical shells based on Winkler-Pasternak elastic foundation by using the GDQ method.

The new contribution of that paper is the investigation by analytical method on the buckling behavior of shell taking into account the change in distance between stringers in the meridional direction. The important highlight is that the authors used the smeared stiffeners technique for correctly establishing the general formula for force and moment resultants of eccentrically stiffened FGM (ES-FGM) truncated conical shells.

2 PROBLEM DESCRIPTION

2.1 Functionally graded material properties

In this section, the aim is to obtain the buckling equations of the cone shell made of porous materials in Fig. 1, in which x is along the edges of the cone, θ is in the direction of the medium, and z is in line with the thickness of the crust. The displacements (u, v, w) are in line (x, θ, z), respectively. Also the cone angle that can vary from zero to 90 degrees.

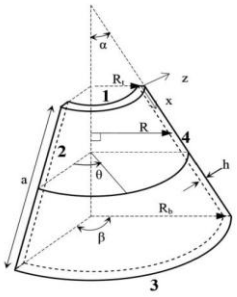

Fig.1
Geometrical shape.

In this paper, we obtain equilibrium equations and conical shell stability equations using the Euler and Trefftz equations. In Figs. (2) and (3) two different types of distribution of porous material are shown along the thickness direction.

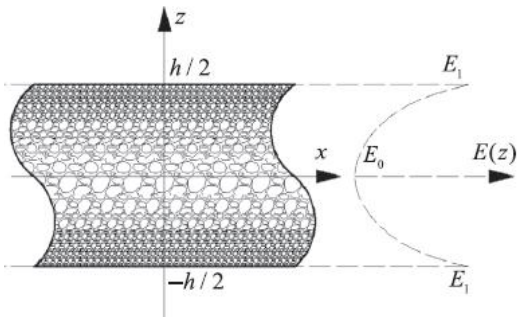

Fig.2
Porosity Distribution 1.

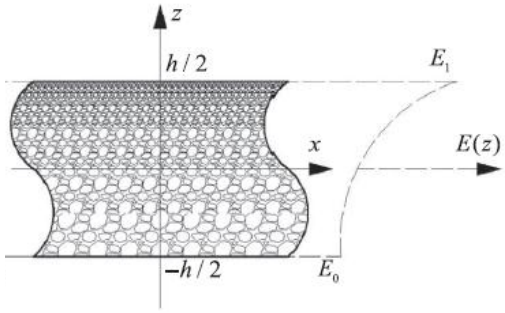

Fig.3
Porosity Distribution 1.

Due to the non-uniform distribution of porous materials in the direction of the thickness of the modulus of elasticity and the shear modulus, they change as a function of z in relations (1) to (2). In type 1 distribution, the lowest values are related to the modulus of elasticity and shear modulus in the middle of the shell and the highest values are related to the modulus of elasticity and shear modulus in the upper and lower sides of the crust, but in the type 2 distribution, the lowest values belong to the modulus of elasticity and modulus The shear is located on the bottom of the shell, and the largest values are the modulus of elasticity and shear modulus on the top of the shell.

The relations of elastic modulus $E(z)$ and shear modulus $G(z)$ for the porous materials anent distribution type 1 and type 2 are obtained as follows.

$$\begin{aligned} &porosity\ \ distribution\ 1: \\ &E(z) = E_1\left[1 - e_0\cos(\pi\varsigma)\right] \\ &G(z) = G_1\left[1 - e_0\cos(\pi\varsigma)\right] \end{aligned} \tag{1}$$

porosity distribution 2 :

$$E(z)=E_1\left[1-e_0\cos\left(\frac{\pi}{2}\varsigma+\frac{\pi}{4}\right)\right]$$
$$G(z)=G_1\left[1-e_0\cos\left(\frac{\pi}{2}\varsigma+\frac{\pi}{4}\right)\right] \quad (2)$$
$$\alpha(z)=\alpha_1\left[1-e_0\cos\left(\frac{\pi}{2}\varsigma+\frac{\pi}{4}\right)\right]$$

In the above relations $\varsigma=\frac{z}{h}$. The displacement coefficient is also equal to $e_0=1-\frac{E_0}{E_1}=1-\frac{G_0}{G_1}$. For isotropic materials, the elastic modulus *E* and the shear modulus *G* are as follows.

$$G_i=\frac{E_i}{2(1+\nu)} \quad i=0,1 \quad (3)$$

2.2 The basic formulation

The relation of the classical displacement field for double curved shell is as follows.

$$u_1(x,\theta,z)=u(x,\theta)+z\,\beta_1(x,\theta)$$
$$u_2(x,\theta,z)=v(x,\theta)+z\,\beta_2(x,\theta) \quad (4)$$
$$u_3(x,\theta,z)=w(x,\theta)$$

In the aforementioned relation, β_1,β_2 are the curvatures of the shell in line with x,θ directions, which according to the assumptions of the Donnell, are expressed as follows. As shown in Fig. 1, $R(x)=x.\sin(\alpha)$.

$$\beta_1=-\frac{\partial w}{\partial x}$$
$$\beta_2=\frac{v.\cos(\alpha)}{R(x)}-\frac{1}{R(x)}\frac{\partial w}{\partial\theta} \quad (5)$$
$$\beta_3=\frac{1}{2R(x)}\left[v.\sin(\alpha)+R(x).\frac{\partial v}{\partial x}-\frac{\partial u}{\partial\theta}\right]$$

Now, by instituting the relations (5) into the relations (4), the classical displacement field relations for the conical shell are obtained using the Donnell assumptions as follows.

$$u_1(x,\theta,z)=u(x,\theta)-z\,\frac{\partial w}{\partial x}$$
$$u_2(x,\theta,z)=v(x,\theta)+z\left(\frac{v.\cos(\alpha)}{R(x)}-\frac{1}{R(x)}\frac{\partial w}{\partial\theta}\right) \quad (6)$$
$$u_3(x,\theta,z)=w(x,\theta)$$

The linear and nonlinear components of normal and shear strains for the conical shell are obtained as follows [2,3] by using the classical displacement field for the conical shell, the Donnell assumptions , the values of the Lame constants and the curvature radii of the conical shell.

$$
\begin{aligned}
&\varepsilon_1 = \varepsilon_x = \frac{\partial u}{\partial x} + \frac{1}{2}\left(\frac{\partial w}{\partial x}\right)^2 \\
&\kappa_1 = \kappa_x = -\frac{\partial^2 w}{\partial x^2} \\
&\varepsilon_2 = \varepsilon_\theta = \frac{1}{R(x)}\frac{\partial v}{\partial \theta} + \frac{u.\sin(\alpha)}{R(x)} + \frac{w.\cos(\alpha)}{R(x)} + \frac{1}{2R^2(x)}\left(\frac{\partial w}{\partial \theta}\right)^2 \\
&\kappa_2 = \kappa_\theta = \frac{1}{R^2(x)}\frac{\partial v}{\partial \theta}\cos(\alpha) - \frac{1}{R^2(x)}\frac{\partial^2 w}{\partial \theta^2} - \frac{\sin(\alpha)}{R(x)}\frac{\partial w}{\partial x} \\
&\gamma_{12} = \gamma_{x\theta} = \frac{\partial v}{\partial x} - \frac{v.\sin(\alpha)}{R(x)} + \frac{1}{R(x)}\frac{\partial u}{\partial \theta} + \frac{1}{R(x)}\left(\frac{\partial w}{\partial x}\right)\left(\frac{\partial w}{\partial \theta}\right) \\
&\kappa_{12} = \kappa_{x\theta} = \frac{3}{2}\frac{\cos(\alpha)}{R(x)}\frac{\partial v}{\partial x} - \frac{3}{2}\frac{\sin(\alpha).\cos(\alpha)}{R^2(x)}v + \frac{2.\sin(\alpha)}{R^2(x)}\frac{\partial w}{\partial \theta} - \frac{2}{R(x)}\frac{\partial^2 w}{\partial x\,\partial \theta} - \frac{1}{2}\frac{\cos(\alpha)}{R^2(x)}\frac{\partial u}{\partial \theta} \\
&\kappa_{12} = \kappa_{x\theta} = \frac{\cos(\alpha)}{R(x)}\frac{\partial v}{\partial x} - 2\frac{\sin(\alpha).\cos(\alpha)}{R^2(x)}v + \frac{2.\sin(\alpha)}{R^2(x)}\frac{\partial w}{\partial \theta} - \frac{2}{R(x)}\frac{\partial^2 w}{\partial x\,\partial \theta}
\end{aligned}
\tag{7}
$$

The linear components of the normal thermal strain for the conical shell are as follows.

$$
\begin{aligned}
&\varepsilon_1^T = \varepsilon_x^T = -\alpha_x \Delta T \\
&\varepsilon_2^T = \varepsilon_\theta^T = -\alpha_\theta \Delta T
\end{aligned}
\tag{8}
$$

Now we want to obtain the equilibrium equations of the conical shell under the external force using Euler's equations. The total potential energy for the cone shell is defined as follows.

$$
\begin{aligned}
&\Pi = U + V \\
&U = \frac{1}{2}\int \sigma_{ij}\varepsilon_{ij} dV \Rightarrow \delta U = \int \sigma_{ij}\delta\varepsilon_{ij} dV \\
&V = \frac{1}{2}\int F_i u_i dV \Rightarrow \delta V = \int F_i \delta u_i dV
\end{aligned}
\tag{9}
$$

In the above relation, U is the strain energy of the system and V is the external work of the external forces entering the system. For the conical shell, the external work obtained from the elastic bed forces is obtained in the form below.

$$
\begin{aligned}
&q_e = k_1 w - k_2 \nabla^2 w = k_1 w - k_2\left(\frac{\partial^2 w}{\partial x^2} + \frac{1}{x}\frac{\partial w}{\partial x} + \frac{1}{x^2}\frac{\partial^2 w}{\partial \theta^2}\right) \\
&V = \frac{1}{2}\int q_e w dV = \frac{1}{2}\int_\theta\int_x \left(k_1 w - k_2 \nabla^2 w\right) w R(x) dx d\theta
\end{aligned}
\tag{10}
$$

In the above relation, k_1 is the Winkler coefficient and k_2 is the Pasternak coefficient. In addition, for the cone crust, the strain energy is obtained in the form below.

$$
\begin{aligned}
&U = \frac{1}{2}\int_V \sigma_{ij}\varepsilon_{ij} dV \\
&U = \frac{1}{2}\int_z\int_\theta\int_x \left\{\sigma_x \varepsilon_x + \sigma_\theta \varepsilon_\theta + \sigma_{x\theta}\gamma_{x\theta}\right\} R(x) dx d\theta dz
\end{aligned}
\tag{11}
$$

To simplify the relationship between the strain energy, we define the forces and flexural torques below [1]

$$[N, M]_{ij} = \int_{-h/2}^{h/2} \sigma_{ij}(1, z)\, dz \tag{12}$$

where N is the membrane force and M is the bending torque. By substituting the resultant stress Eq. (12) in the strain energy Eq. (11) we have:

$$U = \frac{1}{2}\int_{\theta}\int_{x}\left\{\begin{array}{l} N_x.R(x)\dfrac{\partial u}{\partial x}+\dfrac{1}{2}N_x.R(x)\left(\dfrac{\partial w}{\partial x}\right)^2-M_x.R(x)\dfrac{\partial^2 w}{\partial x^2}+N_\theta\dfrac{\partial v}{\partial \theta}+N_\theta u.\sin(\alpha)+N_\theta w.\cos(\alpha)+\dfrac{1}{2}\dfrac{N_\theta}{R(x)}\left(\dfrac{\partial w}{\partial \theta}\right)^2 \\ +M_\theta\dfrac{\cos(\alpha)}{R(x)}\dfrac{\partial v}{\partial \theta}-\dfrac{M_\theta}{R(x)}\dfrac{\partial^2 w}{\partial \theta^2}-M_\theta.\sin(\alpha)\dfrac{\partial w}{\partial x}+N_{x\theta}.R(x)\dfrac{\partial v}{\partial x}-N_{x\theta}v.\sin(\alpha)+N_{x\theta}\dfrac{\partial u}{\partial \theta}+N_{x\theta}\left(\dfrac{\partial w}{\partial x}\right)\left(\dfrac{\partial w}{\partial \theta}\right) \\ +\dfrac{3}{2}M_{x\theta}.\cos(\alpha)\dfrac{\partial v}{\partial x}-\dfrac{3}{2}M_{x\theta}\dfrac{\sin(\alpha).\cos(\alpha)}{R(x)}v+2M_{x\theta}\dfrac{\sin(\alpha)}{R(x)}\dfrac{\partial w}{\partial \theta}-2M_{x\theta}\dfrac{\partial^2 w}{\partial x\,\partial \theta}-\dfrac{1}{2}M_{x\theta}\dfrac{\cos(\alpha)}{R(x)}\dfrac{\partial u}{\partial \theta} \end{array}\right\} dx\,d\theta \tag{13}$$

Now, using the following equation, you can obtain the total functional. [4]

$$\Pi = \frac{1}{2}\int_{\theta}\int_{x} F(x,\theta)\,dx\,d\theta \tag{14}$$

Using Eq. (14) we have:

$$\begin{array}{l} F(x,\theta) = N_x.R(x)\dfrac{\partial u}{\partial x}+\dfrac{1}{2}N_x.R(x)\left(\dfrac{\partial w}{\partial x}\right)^2-M_x.R(x)\dfrac{\partial^2 w}{\partial x^2}+N_\theta\dfrac{\partial v}{\partial \theta}+N_\theta u.\sin(\alpha)+N_\theta w.\cos(\alpha)+\dfrac{1}{2}\dfrac{N_\theta}{R(x)}\left(\dfrac{\partial w}{\partial \theta}\right)^2+M_\theta\dfrac{\cos(\alpha)}{R(x)}\dfrac{\partial v}{\partial \theta} \\ -\dfrac{M_\theta}{R(x)}\dfrac{\partial^2 w}{\partial \theta^2}-M_\theta.\sin(\alpha)\dfrac{\partial w}{\partial x}+N_{x\theta}.R(x)\dfrac{\partial v}{\partial x}-N_{x\theta}v.\sin(\alpha)+N_{x\theta}\dfrac{\partial u}{\partial \theta}+N_{x\theta}\left(\dfrac{\partial w}{\partial x}\right)\left(\dfrac{\partial w}{\partial \theta}\right)+\dfrac{3}{2}M_{x\theta}.\cos(\alpha)\dfrac{\partial v}{\partial x}-\dfrac{3}{2}M_{x\theta}\dfrac{\sin(\alpha).\cos(\alpha)}{R(x)}v \\ +2M_{x\theta}\dfrac{\sin(\alpha)}{R(x)}\dfrac{\partial w}{\partial \theta}-2M_{x\theta}\dfrac{\partial^2 w}{\partial x\,\partial \theta}-\dfrac{1}{2}M_{x\theta}\dfrac{\cos(\alpha)}{R(x)}\dfrac{\partial u}{\partial \theta}+\dfrac{1}{2}k_1.R(x)w^2-k_2 w.R(x).\left(\dfrac{\partial^2 w}{\partial x^2}+\dfrac{1}{x}\dfrac{\partial w}{\partial x}+\dfrac{1}{x^2}\dfrac{\partial^2 w}{\partial \theta^2}\right) \end{array} \tag{15}$$

Now we use the Euler equation method to obtain equations of equilibrium as follows:

$$\begin{array}{l} \dfrac{\partial F}{\partial u}-\dfrac{\partial}{\partial x}\dfrac{\partial F}{\partial u_{,x}}-\dfrac{\partial}{\partial \theta}\dfrac{\partial F}{\partial u_{,\theta}}=0 \\ \dfrac{\partial F}{\partial v}-\dfrac{\partial}{\partial x}\dfrac{\partial F}{\partial v_{,x}}-\dfrac{\partial}{\partial \theta}\dfrac{\partial F}{\partial v_{,\theta}}=0 \\ \dfrac{\partial F}{\partial w}-\dfrac{\partial}{\partial x}\dfrac{\partial F}{\partial w_{,x}}-\dfrac{\partial}{\partial \theta}\dfrac{\partial F}{\partial w_{,\theta}}+\dfrac{\partial^2}{\partial x^2}\dfrac{\partial F}{\partial w_{,xx}}+\dfrac{\partial^2}{\partial x\,\partial \theta}\dfrac{\partial F}{\partial w_{,x\theta}}+\dfrac{\partial^2}{\partial \theta^2}\dfrac{\partial F}{\partial w_{,\theta\theta}}=0 \end{array} \tag{16}$$

Within calculating each term of the above equations, the equilibrium equations of cylindrical shell are obtained by considering the classical model of surfaces and Donnell assumptions. As seen from the above equations, the conical shell equilibrium equations are non-linear.

$$\begin{array}{l} N_\theta.\sin(\alpha)-\dfrac{\partial}{\partial x}\left(N_x.R(x)\right)-\dfrac{\partial}{\partial \theta}\left(N_{x\theta}-\dfrac{1}{2}M_{x\theta}\dfrac{\cos(\alpha)}{R(x)}\right)=0 \\ -N_{x\theta}.\sin(\alpha)-\dfrac{3}{2}M_{x\theta}\dfrac{\sin(\alpha).\cos(\alpha)}{R(x)}-\dfrac{\partial}{\partial x}\left(N_{x\theta}.R(x)+\dfrac{3}{2}M_{x\theta}.\cos(\alpha)\right)-\dfrac{\partial}{\partial \theta}\left(N_\theta+M_\theta\dfrac{\cos(\alpha)}{R(x)}\right)=0 \\ N_\theta.\cos(\alpha)-\dfrac{\partial}{\partial x}\left(N_x.R(x)\left(\dfrac{\partial w}{\partial x}\right)-M_\theta.\sin(\alpha)+N_{x\theta}\left(\dfrac{\partial w}{\partial \theta}\right)\right)-\dfrac{\partial}{\partial \theta}\left(\dfrac{N_\theta}{R(x)}\left(\dfrac{\partial w}{\partial \theta}\right)+2M_{x\theta}\dfrac{\sin(\alpha)}{R(x)}+N_{x\theta}\left(\dfrac{\partial w}{\partial x}\right)\right) \\ -\dfrac{\partial^2}{\partial x^2}\left(M_x.R(x)\right)-2\dfrac{\partial^2}{\partial x\,\partial \theta}\left(M_{x\theta}\right)-\dfrac{\partial^2}{\partial \theta^2}\left(\dfrac{M_\theta}{R(x)}\right)+R(x).k_1 w-R(x).k_2\left(\dfrac{\partial^2 w}{\partial x^2}+\dfrac{1}{x}\dfrac{\partial w}{\partial x}+\dfrac{1}{R^2(x)}\dfrac{\partial^2 w}{\partial \theta^2}\right)=0 \end{array} \tag{17}$$

In order to obtain equations of equilibrium in terms of displacement, we must obtain the tensile vibrations by using Hooke's law in terms of displacements. The stress-strain relationship under stress condition for isotropic materials is as follows:

$$\begin{Bmatrix}\sigma_1\\ \sigma_2\\ \sigma_3\\ \sigma_4\\ \sigma_5\\ \sigma_6\end{Bmatrix}=\begin{bmatrix}Q_{11} & Q_{12} & 0 & 0 & 0 & 0\\ Q_{12} & Q_{22} & 0 & 0 & 0 & 0\\ 0 & 0 & 0 & 0 & 0 & 0\\ 0 & 0 & 0 & Q_{44} & 0 & 0\\ 0 & 0 & 0 & 0 & Q_{55} & 0\\ 0 & 0 & 0 & 0 & 0 & Q_{66}\end{bmatrix}\begin{Bmatrix}\varepsilon_1-\alpha_1\Delta T\\ \varepsilon_2-\alpha_2\Delta T\\ \varepsilon_3\\ \varepsilon_4\\ \varepsilon_5\\ \varepsilon_6\end{Bmatrix} \tag{18}$$

The tensions are defined as follows.

$$\begin{aligned}\sigma_1&=\sigma_{xx} & \sigma_4&=\sigma_{\theta z}\\ \sigma_2&=\sigma_{\theta\theta} & \sigma_5&=\sigma_{xz}\\ \sigma_3&=\sigma_{zz} & \sigma_6&=\sigma_{x\theta}\end{aligned} \tag{19}$$

The stiffness coefficients of matrix Q for porous materials are also defined by:

$$\begin{aligned}&Q_{11}(z)=Q_{22}(z)=\frac{E(z)}{1-\nu^2}\\ &Q_{12}(z)=\frac{E(z)\nu}{1-\nu^2}\\ &Q_{66}(z)=G(z)\end{aligned} \tag{20}$$

In the above relation, the elasticity and shear modulus functions are defined in Eq. (2). By inserting the stiffness matrix components within the Hooke relationship, the Cauchy stress components are obtained as follows:

$$\begin{aligned}\sigma_x&=Q_{11}(z)\varepsilon_x+Q_{12}(z)\varepsilon_\theta-Q_{11}(z)\varepsilon_x^T-Q_{12}(z)\varepsilon_\theta^T\\ \sigma_\theta&=Q_{12}(z)\varepsilon_x+Q_{22}(z)\varepsilon_\theta-Q_{12}(z)\varepsilon_x^T-Q_{22}(z)\varepsilon_\theta^T\\ \sigma_{x\theta}&=Q_{66}(z)\gamma_{x\theta}\end{aligned} \tag{21}$$

The tensile and flexural stiffness matrices are also defined as follows. [12]

$$[A,B,D]_{ij}=\int_{-h/2}^{h/2}Q_{ij}(z)\left(1,z,z^2\right)dz \tag{22}$$

where A is the tensile stiffness matrix, and B is the matrix of the bending-tensile coupling stiffness, and D, is the flexural stiffness matrix.Thermal stiffness matrices are:

$$\begin{aligned}[\varphi_x,\varphi_\theta]_{ij}&=\int_{-h/2}^{h/2}Q_{ij}(z)(\alpha_x,\alpha_\theta)\Delta T dz\\ [\eta_x,\eta_\theta]_{ij}&=\int_{-h/2}^{h/2}zQ_{ij}(z)(\alpha_x,\alpha_\theta)\Delta T dz\end{aligned} \tag{23}$$

Using the relations (12) and (21-23), we can write the membrane force sequences in terms of displacement terms.

$$
\begin{aligned}
&M_x = B_{11}\frac{\partial u}{\partial x}+\frac{B_{11}}{2}\left(\frac{\partial w}{\partial x}\right)^2 - D_{11}\frac{\partial^2 w}{\partial x^2}+\frac{B_{12}}{R(x)}\frac{\partial v}{\partial \theta}+B_{12}\frac{u.\sin(\alpha)}{R(x)}+B_{12}\frac{w.\cos(\alpha)}{R(x)}+\frac{B_{12}}{2R^2(x)}\left(\frac{\partial w}{\partial \theta}\right)^2\\
&+D_{12}\frac{1}{R^2(x)}\frac{\partial v}{\partial \theta}\cos(\alpha)-D_{12}\frac{1}{R^2(x)}\frac{\partial^2 w}{\partial \theta^2}-D_{12}\frac{\sin(\alpha)}{R(x)}\frac{\partial w}{\partial x}-\eta_{x11}-\eta_{\theta 12}\\
&M_\theta = B_{12}\frac{\partial u}{\partial x}+\frac{B_{12}}{2}\left(\frac{\partial w}{\partial x}\right)^2 - D_{12}\frac{\partial^2 w}{\partial x^2}+\frac{B_{22}}{R(x)}\frac{\partial v}{\partial \theta}+B_{22}\frac{u.\sin(\alpha)}{R(x)}+B_{22}\frac{w.\cos(\alpha)}{R(x)}+\frac{B_{22}}{2R^2(x)}\left(\frac{\partial w}{\partial \theta}\right)^2\\
&+D_{22}\frac{1}{R^2(x)}\frac{\partial v}{\partial \theta}\cos(\alpha)-D_{22}\frac{1}{R^2(x)}\frac{\partial^2 w}{\partial \theta^2}-D_{22}\frac{\sin(\alpha)}{R(x)}\frac{\partial w}{\partial x}-\eta_{x12}-\eta_{\theta 22}\\
&M_{x\theta} = B_{66}\frac{\partial v}{\partial x}-B_{66}\frac{v.\sin(\alpha)}{R(x)}+\frac{B_{66}}{R(x)}\frac{\partial u}{\partial \theta}+\frac{B_{66}}{R(x)}\left(\frac{\partial w}{\partial x}\right)\left(\frac{\partial w}{\partial \theta}\right)+D_{66}\frac{3}{2}\frac{\cos(\alpha)}{R(x)}\frac{\partial v}{\partial x}-D_{66}\frac{3}{2}\frac{\sin(\alpha).\cos(\alpha)}{R^2(x)}v\\
&+D_{66}\frac{2.\sin(\alpha)}{R^2(x)}\frac{\partial w}{\partial \theta}-D_{66}\frac{2}{R(x)}\frac{\partial^2 w}{\partial x\,\partial \theta}-D_{66}\frac{1}{2}\frac{\cos(\alpha)}{R^2(x)}\frac{\partial u}{\partial \theta}
\end{aligned}
\tag{24}
$$

To get the equilibrium equations in terms of displacement, the above resultant stresses should be inserted within the equilibrium equations.

3 THE EQUILIBRIUM EQUATIONS OF CONICAL SHELL BASED ON TREFFTZ PRINCIPLE

The equilibrium equations of conical shell are derived based on neighboring equilibrium ratio (adjacent) in equipoise equilibrium state or Trefftz principle. It is considered that, equivalence condition of conical shell are presented under the thermal field in terms of u_0, v_0, w_0 components. The equipoise equilibrium state is alluded on basis of infinitesimal virtual components u_1, v_1, w_1. The total displacement components in the equipoise state are as follows.

$$
\begin{aligned}
u &= u_0 + u_1\\
v &= v_0 + v_1\\
w &= w_0 + w_1
\end{aligned}
\tag{25}
$$

Similar to the above, the forces and bending moments are expressed in terms of the sum of equilibrium and neighbor states.

$$
\begin{aligned}
N_x &= N_x^0 + N_x^1\\
N_\theta &= N_\theta^0 + N_\theta^1\\
N_{x\theta} &= N_{x\theta}^0 + N_{x\theta}^1\\
M_x &= M_x^0 + M_x^1\\
M_\theta &= M_\theta^0 + M_\theta^1\\
M_{x\theta} &= M_{x\theta}^0 + M_{x\theta}^1
\end{aligned}
\tag{26}
$$

The subtitle terms 0 are related to displacements u_0, v_0, w_0, and the subtitle terms 1 are associated with displacements u_1, v_1, w_1, which express the additional part of the forces and torque outputs that are in linear u_1, v_1, w_1 terms . By entering Eqs. (25) and (26) in 17, the terms of the equations obtained with the index 0 satisfy the equilibrium conditions. So, they are eliminated from equilibrium stability equations. Then, the stability equations

are obtained by ignoring nonlinear terms (second-order semantics) in u_1, v_1, w_1 due to their infinitesimal size to the linear terms and the rest of the components of $N_x^1, N_\theta^1, \ldots$.

$$
\begin{aligned}
&N_\theta^1.\sin(\alpha)-\frac{\partial}{\partial x}\left(N_x^1.R(x)\right)-\frac{\partial}{\partial\theta}\left(N_{x\theta}^1-\frac{1}{2}M_{x\theta}^1\frac{\cos(\alpha)}{R(x)}\right)=0\\
&-N_{x\theta}^1.\sin(\alpha)-\frac{3}{2}M_{x\theta}^1\frac{\sin(\alpha).\cos(\alpha)}{R(x)}-\frac{\partial}{\partial x}\left(N_{x\theta}^1.R(x)+\frac{3}{2}M_{x\theta}^1.\cos(\alpha)\right)-\frac{\partial}{\partial\theta}\left(N_\theta^1+M_\theta^1\frac{\cos(\alpha)}{R(x)}\right)=0\\
&N_\theta^1.\cos(\alpha)-\frac{\partial}{\partial x}\left(N_x^0.R(x)\left(\frac{\partial w}{\partial x}\right)-M_\theta^1.\sin(\alpha)+N_{x\theta}^0\left(\frac{\partial w}{\partial\theta}\right)\right)-\frac{\partial}{\partial\theta}\left(\frac{N_\theta^0}{R(x)}\left(\frac{\partial w}{\partial\theta}\right)+2M_{x\theta}^1\frac{\sin(\alpha)}{R(x)}+N_{x\theta}^0\left(\frac{\partial w}{\partial x}\right)\right)\\
&+\frac{\partial^2}{\partial x^2}\left(-M_x^1.R(x)\right)+\frac{\partial^2}{\partial x\,\partial\theta}\left(-2M_{x\theta}^1\right)+\frac{\partial^2}{\partial\theta^2}\left(-\frac{M_\theta^1}{R(x)}\right)+R(x).k_1w-R(x).k_2\left(\frac{\partial^2w}{\partial x^2}+\frac{1}{x}\frac{\partial w}{\partial x}+\frac{1}{R^2(x)}\frac{\partial^2w}{\partial\theta^2}\right)=0
\end{aligned}
\tag{27}
$$

In the above equations, N_x^0 is the axial thermal buckling force.

$$
\begin{aligned}
&N_x=\int_{-h/2}^{h/2}\sigma_x^T dz=\int_{-h/2}^{h/2}\left[-Q_{11}(z)\varepsilon_x^T-Q_{12}(z)\varepsilon_\theta^T\right]dz\\
&=\int_{-h/2}^{h/2}\left[-Q_{11}(z)\alpha_x\Delta T-Q_{12}(z)\alpha_\theta\Delta T\right]dz=-\varphi_{x11}-\varphi_{\theta12}
\end{aligned}
\tag{28}
$$

In addition, the resultant stresses associated with the small development of the neighborhood are obtained as follows, regardless of nonlinear regions.

$$
\begin{aligned}
&N_x^1=A_{11}\frac{\partial u}{\partial x}-B_{11}\frac{\partial^2w}{\partial x^2}+\frac{A_{12}}{R(x)}\frac{\partial v}{\partial\theta}+A_{12}\frac{u.\sin(\alpha)}{R(x)}+A_{12}\frac{w.\cos(\alpha)}{R(x)}+B_{12}\frac{1}{R^2(x)}\frac{\partial v}{\partial\theta}\cos(\alpha)\\
&-B_{12}\frac{1}{R^2(x)}\frac{\partial^2w}{\partial\theta^2}-B_{12}\frac{\sin(\alpha)}{R(x)}\frac{\partial w}{\partial x}-\varphi_{x11}-\varphi_{\theta12}\\
&N_\theta^1=A_{12}\frac{\partial u}{\partial x}-B_{12}\frac{\partial^2w}{\partial x^2}+\frac{A_{22}}{R(x)}\frac{\partial v}{\partial\theta}+A_{22}\frac{u.\sin(\alpha)}{R(x)}+A_{22}\frac{w.\cos(\alpha)}{R(x)}+B_{22}\frac{1}{R^2(x)}\frac{\partial v}{\partial\theta}\cos(\alpha)\\
&-B_{22}\frac{1}{R^2(x)}\frac{\partial^2w}{\partial\theta^2}-B_{22}\frac{\sin(\alpha)}{R(x)}\frac{\partial w}{\partial x}-\varphi_{x12}-\varphi_{\theta22}\\
&N_{x\theta}^1=A_{66}\frac{\partial v}{\partial x}-A_{66}\frac{v.\sin(\alpha)}{R(x)}+\frac{A_{66}}{R(x)}\frac{\partial u}{\partial\theta}+B_{66}\frac{3}{2}\frac{\cos(\alpha)}{R(x)}\frac{\partial v}{\partial x}-B_{66}\frac{3}{2}\frac{\sin(\alpha).\cos(\alpha)}{R^2(x)}v\\
&+B_{66}\frac{2.\sin(\alpha)}{R^2(x)}\frac{\partial w}{\partial\theta}-B_{66}\frac{2}{R(x)}\frac{\partial^2w}{\partial x\,\partial\theta}-B_{66}\frac{1}{2}\frac{\cos(\alpha)}{R^2(x)}\frac{\partial u}{\partial\theta}\\
&M_x^1=B_{11}\frac{\partial u}{\partial x}-D_{11}\frac{\partial^2w}{\partial x^2}+\frac{B_{12}}{R(x)}\frac{\partial v}{\partial\theta}+B_{12}\frac{u.\sin(\alpha)}{R(x)}+B_{12}\frac{w.\cos(\alpha)}{R(x)}+D_{12}\frac{1}{R^2(x)}\frac{\partial v}{\partial\theta}\cos(\alpha)\\
&-D_{12}\frac{1}{R^2(x)}\frac{\partial^2w}{\partial\theta^2}-D_{12}\frac{\sin(\alpha)}{R(x)}\frac{\partial w}{\partial x}-\eta_{x11}-\eta_{\theta12}\\
&M_\theta^1=B_{12}\frac{\partial u}{\partial x}-D_{12}\frac{\partial^2w}{\partial x^2}+\frac{B_{22}}{R(x)}\frac{\partial v}{\partial\theta}+B_{22}\frac{u.\sin(\alpha)}{R(x)}+B_{22}\frac{w.\cos(\alpha)}{R(x)}+D_{22}\frac{1}{R^2(x)}\frac{\partial v}{\partial\theta}\cos(\alpha)\\
&-D_{22}\frac{1}{R^2(x)}\frac{\partial^2w}{\partial\theta^2}-D_{22}\frac{\sin(\alpha)}{R(x)}\frac{\partial w}{\partial x}-\eta_{x12}-\eta_{\theta22}\\
&M_{x\theta}^1=B_{66}\frac{\partial v}{\partial x}-B_{66}\frac{v.\sin(\alpha)}{R(x)}+\frac{B_{66}}{R(x)}\frac{\partial u}{\partial\theta}+D_{66}\frac{3}{2}\frac{\cos(\alpha)}{R(x)}\frac{\partial v}{\partial x}-D_{66}\frac{3}{2}\frac{\sin(\alpha).\cos(\alpha)}{R^2(x)}v+D_{66}\frac{2.\sin(\alpha)}{R^2(x)}\frac{\partial w}{\partial\theta}\\
&-D_{66}\frac{2}{R(x)}\frac{\partial^2w}{\partial x\,\partial\theta}-D_{66}\frac{1}{2}\frac{\cos(\alpha)}{R^2(x)}\frac{\partial u}{\partial\theta}
\end{aligned}
\tag{29}
$$

By placing the above-mentioned stress factors in the stability Eqs. (27), they are obtained in terms of displacement terms.

3.1 Solving equations by differential quadrature method

Primarily, we consider conical shell displacements in the following geometric relation due to the existence of axial symmetry to solve the equilibrium equations,

$$\begin{aligned} u(x,\theta) &= u(x)\cos(n\theta) \\ v(x,\theta) &= v(x)\sin(n\theta) \\ w(x,\theta) &= w(x)\cos(n\theta) \end{aligned} \tag{30}$$

In the above relation, n is the number of environmental waves that we consider to find the critical buckling force equal to $n = 1$. In order to solve the differential equations, we use the generalized differential Quadrature method.

3.2 Principles of differential quadrature method and generalized differential quadrature

The differential quadrature method, or DQ, is a powerful method for solving initial or boundary value problems. Richard Bellman developed this technique in the early seventies of the twentieth century. The main idea in the DQ method is the approximation of the unknown function and its derivatives in each node as a linear sum of the function values in all nodes in the interval under consideration. In this method, the derivative of the nth order approximates the smooth function over the node as follows.

$$\left.\frac{df(x)}{dx}\right|_{x=x_i} = \sum_{j=1}^{N} C_{ij}^{(1)} f(x_j) \quad i = 1,2,...,N \tag{31}$$

An important point in the DQ method is the way of choosing the weight coefficient and the distribution of the discontinuity points. The differential quadrature method was determined by Shu in the early 1990s to improve the DQ method in determining the weight coefficients [13]. The principles of this method are similar to the DQ method, but the weight coefficients determination is different. In GDQ method, the weight coefficient for the first-order derivative is obtained by a simple algebraic relation. The weight coefficients for higher order derivatives are also determined by a recurrence relation. The first-order derivative weigh coefficients are gained as the following relationships [13]:

$$C_{ij}^{(1)} = \frac{M(x_i)}{(x_i - x_j)M(x_j)} \quad ,i \neq j \tag{32}$$

where

$$M(x_i) = \prod_{j=1, j\neq i}^{N} (x_i - x_j) \tag{33}$$

which $x_1, x_2, ..., x_N$ are coordinate nodes and selecting them is optional. The weighting coefficients of the derivative of the m_{th} are calculated from the following recursive relationships:

$$C_{ij}^{(m)} = m\left(C_{ij}^{(1)} C_{ii}^{(m-1)} - \frac{C_{ij}^{(m-1)}}{(x_i - x_j)}\right) \qquad ,i \neq j \tag{34}$$

Similar to the previous state, $C_{ii}^{(m)}$ can be calculated from the following equation:

$$C_{ii}^{(m)} = -\sum_{j=1, j\neq i}^{N} C_{ij}^{(m)} \tag{35}$$

As can be seen, the weight coefficients in the GDQ method do not depend on the studied issue. By choosing the number of discrete points and their distribution, these coefficients are calculated using the above relations. Burt and Malik [14] pointed out that the proper distribution method is dependent on the considered problem, and has proposed the use of Chebyshev –Gauss- Lobatto (C-G-L) distribution for solving mechanical problems of structures due to the high convergence velocity in the results. The distribution of C-G-L is as follows.

$$x_i = \frac{1-\cos\left((i-1)\pi/(N-1)\right)}{2} L \qquad ,i = 1,2,...,N \tag{36}$$

In the above distribution, the density of nodes in the two rows is greater than the median range, and therefore the boundaries of the conditions in this division have a more effective role than the division with equal distances. To apply boundary conditions in the GDQ method, at the boundary point, the boundary condition replaces the equation studied at that point. In some issues, such as the vibration of the beams, there are more than one boundary condition at each boundary. Using the above method, the number of equations generated by the discretization of the GDQ method increases the number of sudden events, which is the same amount of value in the nodes. Different ways have been proposed to solve this problem. One of the methods used in this research is to remove the equation for one of the internal points and replace it with the additional equation obtained by applying the GDQ method to the multiple boundary condition. Shu [15] has shown that this method is very suitable for vibrations of beams and sheets with different boundaries. It has also been shown that the optimal choice for the internal substitute point is the adjacent node of boundary conditions. By replacing the relation (31) within the stability Eqs. (27), it follows from the linear algebraic equation system.

$$\begin{aligned}
&R(x)A_{11}\sum_{j=1}^{n}C_{ij}^{(2)}u_j + A_{12}\sum_{j=1}^{n}C_{ij}^{(1)}v_j - R(x)B_{11}\sum_{j=1}^{n}C_{ij}^{(3)}w_j - \frac{\sin(\alpha)}{R^2(x)}B_{12}w_i + \frac{B_{12}}{R(x)}\sum_{j=1}^{n}C_{ij}^{(1)}w_j - \frac{A_{66}}{R(x)}u_i - 2\frac{\sin(\alpha)}{R^2(x)}B_{66}w_i \\
&+2\frac{B_{66}}{R(x)}\sum_{j=1}^{n}C_{ij}^{(1)}w_j - \frac{\sin(\alpha)}{R(x)}A_{22}v_i - \frac{\sin^2(\alpha)}{R(x)}A_{22}u_i - \frac{\sin(\alpha)}{R^2(x)}B_{22}w_i + \frac{\sin^2(\alpha)}{R(x)}B_{22}\sum_{j=1}^{n}C_{ij}^{(1)}w_j + A_{12}\cos(\alpha)\sum_{j=1}^{n}C_{ij}^{(1)}w_j \\
&-\frac{\sin(\alpha)\cos(\alpha)}{R^2(x)}B_{12}v_i + \frac{\cos(\alpha)}{R(x)}B_{12}\sum_{j=1}^{n}C_{ij}^{(1)}v_j + \frac{\cos(\alpha)}{R(x)}B_{66}\sum_{j=1}^{n}C_{ij}^{(1)}v_j - 2\frac{\sin(\alpha)\cos(\alpha)}{R^2(x)}B_{66}v_i - \frac{\sin(\alpha)\cos(\alpha)}{R(x)}A_{22}w_i \\
&-\frac{\sin(\alpha)\cos(\alpha)}{R^2(x)}B_{22}v_i + A_{11}\sin(\alpha)\sum_{j=1}^{n}C_{ij}^{(1)}u_j - B_{11}\sin(\alpha)\sum_{j=1}^{n}C_{ij}^{(2)}w_j - \frac{\sin(\alpha)}{R(x)}A_{66}v_i + A_{66}\sum_{j=1}^{n}C_{ij}^{(1)}v_j = 0 \\
&-A_{12}\sum_{j=1}^{n}C_{ij}^{(1)}u_j - \frac{\cos(\alpha)}{R(x)}A_{22}w_i - 2\frac{\cos(\alpha)}{R^2(x)}B_{22}v_i - \frac{\cos(\alpha)}{R(x)}B_{12}\sum_{j=1}^{n}C_{ij}^{(1)}u_j - \frac{\sin(\alpha)\cos(\alpha)}{R^2(x)}B_{22}u_i - \frac{\cos^2(\alpha)}{R^2(x)}B_{22}w_i \\
&-\frac{\cos^2(\alpha)}{R^3(x)}D_{22}v_i - \frac{\cos(\alpha)}{R^3(x)}D_{22}w_i + \frac{\sin(\alpha)\cos(\alpha)}{R^2(x)}D_{22}\sum_{j=1}^{n}C_{ij}^{(1)}w_j - \frac{\sin(\alpha)\cos(\alpha)}{R^2(x)}B_{66}u_i - \frac{\sin(\alpha)\cos^2(\alpha)}{R^2(x)}D_{66}\sum_{j=1}^{n}C_{ij}^{(1)}v_j \\
&-\frac{\cos(\alpha)}{R(x)}B_{66}\sum_{j=1}^{n}C_{ij}^{(1)}u_j - A_{66}\sum_{j=1}^{n}C_{ij}^{(1)}u_j + 2\cos(\alpha)B_{66}\sum_{j=1}^{n}C_{ij}^{(2)}v_j - \frac{\sin^2(\alpha)\cos(\alpha)}{R^2(x)}B_{66}v_i - \frac{A_{22}}{R(x)}v_i - \frac{B_{22}}{R^2(x)}w_i \\
&-\frac{\sin^2(\alpha)}{R(x)}A_{66}v_i + \frac{\cos(\alpha)}{R(x)}D_{12}\sum_{j=1}^{n}C_{ij}^{(2)}w_j + \frac{\cos^2(\alpha)}{R(x)}D_{66}\sum_{j=1}^{n}C_{ij}^{(2)}v_j + 2\frac{\cos(\alpha)}{R(x)}D_{66}\sum_{j=1}^{n}C_{ij}^{(2)}w_j - \frac{\sin(\alpha)}{R(x)}A_{66}u_i - \frac{\sin(\alpha)}{R(x)}A_{22}u_i \\
&+\frac{\sin(\alpha)}{R(x)}B_{22}\sum_{j=1}^{n}C_{ij}^{(1)}w_j + \sin(\alpha)A_{66}\sum_{j=1}^{n}C_{ij}^{(1)}v_j + R(x)A_{66}\sum_{j=1}^{n}C_{ij}^{(2)}v_j + 2B_{66}\sum_{j=1}^{n}C_{ij}^{(2)}w_j + B_{12}\sum_{j=1}^{n}C_{ij}^{(2)}w_j = 0 \\
&-2\cos(\alpha)B_{12}w_i - 2\sin(\alpha)B_{11}\sum_{j=1}^{n}C_{ij}^{(2)}u_j + 2\sin(\alpha)D_{11}\sum_{j=1}^{n}C_{ij}^{(3)}w_j + \frac{\cos(\alpha)}{R(x)}A_{22}v_i + \frac{\cos^2(\alpha)}{R(x)}A_{22}w_i + \frac{\cos^2(\alpha)}{R^2(x)}B_{22}v_i \\
&+2\frac{\cos(\alpha)}{R^2(x)}B_{22}w_i - 2\frac{\sin^2(\alpha)\cos(\alpha)}{R^3(x)}D_{22}v_i + \frac{\sin(\alpha)\cos(\alpha)}{R^2(x)}D_{22}\sum_{j=1}^{n}C_{ij}^{(1)}v_j + 4\frac{\sin(\alpha)\cos(\alpha)}{R^2(x)}D_{66}\sum_{j=1}^{n}C_{ij}^{(1)}v_j \\
&-4\frac{\sin^2(\alpha)\cos(\alpha)}{R^3(x)}D_{66}v_i - 2\frac{\sin^2(\alpha)\cos(\alpha)}{R^3(x)}D_{12}v_i + 2\frac{\sin(\alpha)\cos(\alpha)}{R^2(x)}D_{12}\sum_{j=1}^{n}C_{ij}^{(1)}v_j + \frac{\cos(\alpha)}{R^3(x)}D_{22}v_i + 2N_{x\theta}^{0}\frac{\sin(\alpha)}{\cos(\alpha)}\sum_{j=1}^{n}C_{ij}^{(1)}w_j \\
&-N_x^0\sin(\alpha)\sum_{j=1}^{n}C_{ij}^{(1)}w_j + \cos(\alpha)A_{12}\sum_{j=1}^{n}C_{ij}^{(1)}u_j - \frac{\sin^2(\alpha)}{R^2(x)}B_{22}v_i + \frac{\sin(\alpha)}{R(x)}B_{22}\sum_{j=1}^{n}C_{ij}^{(1)}v_j - N_x^0R(x)\sum_{j=1}^{n}C_{ij}^{(2)}w_j
\end{aligned} \tag{37}$$

$$
\begin{aligned}
&-\frac{\sin^2(\alpha)}{R(x)}D_{22}\sum_{j=1}^{n}C_{ij}^{(2)}w_j - R(x)B_{11}\sum_{j=1}^{n}C_{ij}^{(3)}u_j + R(x)D_{11}\sum_{j=1}^{n}C_{ij}^{(4)}w_j - 2\frac{D_{12}}{R(x)}\sum_{j=1}^{n}C_{ij}^{(2)}w_j - 4\frac{D_{66}}{R(x)}\sum_{j=1}^{n}C_{ij}^{(2)}w_j \\
&-2B_{66}\sum_{j=1}^{n}C_{ij}^{(2)}v_j - B_{12}\sum_{j=1}^{n}C_{ij}^{(2)}v_j - \frac{\sin^2(\alpha)\cos(\alpha)}{R^2(x)}B_{22}w_i + \frac{N_\theta^0}{R(x)}w_i + \frac{\sin(\alpha)\cos(\alpha)}{R(x)}A_{22}u_i - \frac{\sin^3(\alpha)}{R^2(x)}B_{22}u_i \\
&+\frac{\sin^2(\alpha)}{R(x)}B_{22}\sum_{j=1}^{n}C_{ij}^{(1)}u_j - 2\frac{\sin^2(\alpha)}{R^3(x)}D_{22}w_i + \frac{\sin^3(\alpha)}{R^2(x)}D_{22}\sum_{j=1}^{n}C_{ij}^{(1)}w_j - 4\frac{\sin^2(\alpha)}{R^3(x)}D_{66}w_i + 4\frac{\sin(\alpha)}{R^2(x)}D_{66}\sum_{j=1}^{n}C_{ij}^{(1)}w_j \\
&-2\frac{\sin^2(\alpha)}{R^3(x)}D_{12}w_i + 2\frac{\sin(\alpha)}{R^2(x)}D_{12}\sum_{j=1}^{n}C_{ij}^{(1)}w_j + 2\frac{B_{66}}{R(x)}\sum_{j=1}^{n}C_{ij}^{(1)}u_j + \frac{B_{12}}{R(x)}\sum_{j=1}^{n}C_{ij}^{(1)}u_j + \frac{B_{22}}{R^2(x)}v_i + \frac{\sin(\alpha)}{R^2(x)}B_{22}u_i \\
&+\frac{1}{R^3(x)}D_{22}w_i - \frac{\cos(\alpha)}{R(x)}D_{12}\sum_{j=1}^{n}C_{ij}^{(2)}v_j - 2\frac{\cos(\alpha)}{R(x)}D_{66}\sum_{j=1}^{n}C_{ij}^{(2)}v_j + R(x).k_1w_i - R(x).k_2\left(\sum_{j=1}^{n}C_{ij}^{(2)}w_j + \frac{1}{x_i}\sum_{j=1}^{n}C_{ij}^{(1)}w_j - \frac{1}{R^2(x)}w_i\right) = 0
\end{aligned}
\tag{37}
$$

By solving this system of linear algebraic equations, the critical temperature of the buckling is obtained.

4 NUMERICAL RESULTS AND DISCUSSION

As stated before, the numerical results presented here are related to conical shells made of porous materials, which are functionally in line with the thickness of the shell.

4.1 Validation

In this section, to determine the accuracy of the solution method, the results are presented for thermal buckling of a functionally graded conical shell under uniform heat load. The properties of the functionally graded materials are obtained using the following equation.

$$(E,\alpha) = (E_m,\alpha_m) + (E_{cm},\alpha_{cm})(\frac{2z+h}{2h})^N$$

The material used in the functionally graded materials is as follows.

Table 1
Basic constituents of FGM conical shell.

	$E(GPa)$	$\rho(kg/m^3)$
M	200	11.7×10^{-6}
C	380	7.4×10^{-6}

The clamped boundary conditions for the conical shell are defined as follows $v = u = M_x = w = 0$ .Boundary conditions are assumed as clamped in validation. The governing equilibrium equations of the shell obtained in Chapter 4 are solved using the differential quadrature method. We considered the number of nodes equal to $N = 20$. To compare the heat buckling analysis of a conical shell under uniform heat load, the results are compared with reference [7] and presented in Tables 1 to 2.

Table 2
Comparison of critical temperature values of FGM cone shell buckling with SS boundary condition.

$\alpha_c \Delta T_{cr} \times 10^3$

$h = 0.01m, \beta = 10^\circ, H/R = 1, K_1 = 0, K_2 = 0$

N	$R/h = 200$		$R/h = 400$
	present	Ref[7]	present
0	2.83	2.78	1.27
0.3	2.49	2.44	1.13
1	2.23	2.22	1.01
5	1.98	1.95	0.92
∞	1.69	1.73	0.84

Table 3
Comparison of critical temperature values of FGM conical shell`s buckling with SS boundary condition.

$\Delta T_{cr}(K)$

$h = 0.0127m, R_{\circ}/h = 100, L = 2R_{\circ}, \alpha = 30^{\circ}, N = 1$

	K_1 (N/m^3)							
	0		2×10^7		3.5×10^7		6×10^7	
K_2 (N/m)	present	Ref[7]	present	Ref[7]	present	Ref[7]	present	Ref[7]
0	206.12	205	210.34	209	213.30	212	218.15	216
2×10^5	210.25	210	214.27	214	217.23	216	222.07	220
3.5×10^5	213.19	212	217.21	215	220.18	218	225.02	222
6×10^5	218.11	217	222.13	221	225.09	223	229.93	228

According to the results of the above-mentioned tables, the differential quadrature (DQ) method used in this study has a good accuracy.

4.2 Material properties of porous materials

The materials used in the porous conical shell are made of steel foam, the properties of which are as follows.

$E_1 = 200 \quad GPa$
$\rho_1 = 7850 \quad kg/m^3$
$\alpha = 11.7E-6 \quad 1/C^0$
$\nu = 0.3$

4.3 The results of thermal buckling analysis of conical shells made of porous materials

In order to solve the equations using the DQ method, the number of nodes are considered to be N = 30. In this section, the results of thermal buckling analysis of conical shells made of porous materials with simple boundary conditions for different porosity coefficients $0 \prec e_0 \prec 1$ are shown. In the below tables, the critical temperature values of the buckling of the conical shell made of porous materials are obtained by simply and clamped supports.

Table 4
Critical temperature values and critical buckling load of porous conical shell with boundary condition SS.

$N_{cr}, \Delta T_{cr}(K)$

SS , *Ra/h*=100 , *L/Ra*=1 , *h*=0.01 , K_1=0 , K_2=0

		$e_0 = 0$		$e_0 = 0.2$		$e_0 = 0.4$		$e_0 = 0.6$		$e_0 = 0.8$	
		Dist. 1	Dist. 2	Dist. 1	Dist. 2	Dist. 1	Dist. 2	Dist. 1	Dist. 2	Dist. 1	Dist. 2
$\alpha = 0$	$\Delta Tcr, Ncr$	349.80	349.80	412.39	400.57	493.14	491.57	591.97	510.89	687.52	523.56
		762.94	762.94	688.41	668.68	613.84	611.89	537.18	463.61	451.97	344.19
$\alpha = 15$	$\Delta Tcr, Ncr$	287.79	287.79	338.48	329.76	403.05	377.36	482.11	422.31	566.07	504.23
		606.31	606.31	545.78	531.70	484.60	453.72	422.59	370.16	359.45	320.18
$\alpha = 30$	$\Delta Tcr, Ncr$	224.92	224.92	264.75	257.87	315.57	295.28	377.88	330.69	443.83	340.50
		424.84	424.84	382.73	372.79	340.18	318.31	296.96	259.88	252.68	193.85
$\alpha = 45$	$\Delta Tcr, Ncr$	166.70	166.70	196.24	191.21	233.97	219.08	280.35	245.52	329.85	253.09
		257.09	257.09	231.63	225.69	205.94	192.83	179.89	157.54	153.33	117.65
$\alpha = 60$	$\Delta Tcr, Ncr$	112.08	112.08	131.98	128.72	157.38	147.72	188.52	165.90	221.62	171.19
		122.23	122.23	110.16	107.44	97.95	91.94	85.53	75.27	72.84	56.27

In Table 3 for comparison, the buckling temperature values along with the critical buckling force of the conical shell made of porous material with a clamped support are obtained. According to the results of the above table, it can be seen that by increasing the porosity coefficient in the porous conical shell with the distribution of type 1 and

2, the amount of critical buckling force decreases and the critical temperature of the buckling increases. Therefore, it is understood that the presence of internal cavities leads to a reduction in the effective stiffened of E and a decrease in the effective permeability coefficient in the shell. The effective reduction of E reduces the amount of buckling force and decreases the effective permeability to increase the critical temperature of buckling in the shell. According to the formula for the porosity coefficient e_0 from Eq. (3), when $e_0 = 0$, the value of E_0 is equal to the value of E_1, and the value of the elastic modulus does not change along the thickness and the matter behaves like isotropic materials. However, if the large cavities were created inside the material, the amount of E_0 will be smaller than E_1 and the porosity coefficient e_0 decreases from 1, and the e_0 value tends to zero as the cavities increase. According to the relation (3), the value of E_0 is approximately zero when the porosity coefficient e_0 is almost equal to zero, which indicates there are too many cavities inside the object.

In addition, according to the results presented in the above tables, we find that the porosity distribution in porous materials with porosity coefficient greater than zero affects the results. In such a way that the critical temperature buckling values in the second-order distribution are always lower than the critical buckling values in the first-order distribution, which is due to the fact that in the first-order distribution of small cavities that are harder than the center, the cylindrical thickness is higher and this causes the hardness of the cylinder to become more effective.

Table 5
Critical buckling temperature values of porous conical shell with boundary condition CC.

$\Delta T_{cr}(K)$

CC , Ra/h=100 , L/Ra=1 , h=0.01, K_1=0 , K_2=0

	$e_0 = 0$		$e_0 = 0.2$		$e_0 = 0.4$		$e_0 = 0.6$		$e_0 = 0.8$	
	Dist. 1	Dist. 2	Dist. 1	Dist. 2	Dist. 1	Dist. 2	Dist. 1	Dist. 2	Dist. 1	Dist. 2
$\alpha = 0$	429.12	429.12	509.73	491.89	608.18	561.83	727.78	624.09	858.28	628.96
$\alpha = 15$	375.51	375.51	401.32	395.75	442.29	411.39	531.01	459.04	625.68	560.16
$\alpha = 30$	322.14	322.14	341.59	338.14	359.67	334.70	431.44	373.41	508.53	471.51
$\alpha = 45$	196.19	196.19	231.57	224.71	277.01	256.77	333.25	286.22	393.73	291.54
$\alpha = 60$	136.83	136.83	161.52	156.72	193.33	179.07	232.96	199.61	276.47	203.31

In addition, according to the results of the above tables, we find that by increasing the angle of the cone in the porous conical shell, the critical temperature of the buckling decreases, which is due to the instability of the cone with a high vertex angle. In the results of the following tables, we show them later in order to better illustrating the effect of geometric dimensions on critical buckling loads.

Table 6
Critical buckling temperature values of porous conical shell with boundary condition SS.

$\Delta T_{cr}(K)$

SS , L/Ra=1 , e_0=0.5 , h=0.01 , Dist. 1, K_1=0 , K_2=0

	$R_a/h = 10$	$R_a/h = 20$	$R_a/h = 50$	$R_a/h = 100$	$R_a/h = 200$
$\alpha = 0$	5602.66	2855.94	1069.03	541.28	267.10
$\alpha = 15$	5025.31	2314.76	903.83	440.97	217.16
$\alpha = 30$	4267.00	1822.95	711.88	345.45	168.55
$\alpha = 45$	3023.74	1412.15	533.02	256.19	124.22
$\alpha = 60$	1923.51	1049.09	361.83	172.31	82.79

From the results above, Table 5, which shows the critical temperature values of the buckling of the porous conical shell with the SS boundary condition, we find that by increasing the vertex angle α , the critical temperature values of the buckling of the conical shell are reduced, which is a natural phenomenon. Because, the increase in the vertex angle α leads the conical shell become geometrically unstable and the buckling phenomenon occurs at a lower temperature.

In addition, from the results of Table 5, it can be seen that by increasing the value of x, the critical temperature values of the buckling of the conical shell decrease, which is due to the fact that by increasing the amount of x the conical shell becomes thinner and its stability is reduced.

Table 7
Critical temperature values of buckling of porous conical shell with boundary condition SS.

$\Delta T_{cr}(K)$

SS , *Ra/h*=100 , e_0=0.5 , *h*=0.01 , Dist. 1, K_1=0 , K_2=0

	$\frac{L}{R_a}=0.2$	$\frac{L}{R_a}=0.5$	$\frac{L}{R_a}=1$	$\frac{L}{R_a}=2$	$\frac{L}{R_a}=5$
$\alpha=0$	568.34	543.02	541.28	533.74	504.65
$\alpha=15$	528.92	499.79	440.97	364.17	267.58
$\alpha=30$	457.18	426.56	345.45	256.13	142.27
$\alpha=45$	372.23	319.88	256.19	178.20	96.84
$\alpha=60$	294.11	224.47	172.31	114.93	72.45

From the results above, Table 6 which shows the critical temperature values of the buckling of the porous conical shell with the SS boundary condition, we comprehend that by increasing L/R_a , the amount of critical temperature values of the buckling of the conical shell is reduced, which is based on a principle that the conical shell becomes longer, and its stability is reduced by increasing the amount of L/R_a .

Table 8
Critical temperature values of buckling of porous cone shell with SS boundary condition in terms of (KN).

$\Delta T_{cr}(K)$

SS , *L/Ra*=1 , *Ra/h*=100 , e_0=0.5 , *h*=0.01*m* , Dist. 1

$\alpha=30$	$K_1=0\times10^7(\frac{N}{m^3})$	$K_1=2\times10^7(\frac{N}{m^3})$	$K_1=4\times10^7(\frac{N}{m^3})$	$K_1=6\times10^7(\frac{N}{m^3})$
$K_2=0\times10^5(N/m)$	345.45	351.68	357.78	363.77
$K_2=2\times10^5(N/m)$	357.25	363.48	369.58	375.56
$K_2=4\times10^5(N/m)$	369.08	375.30	381.40	387.39
$K_2=6\times10^5(N/m)$	380.93	387.15	393.26	399.24

Based on the results above, Table 7, which shows the critical temperature values of the buckling of the porous conical shell with the SS boundary condition, we realize that the critical temperature values of the buckling of the conical shell increase by increasing the elastic foundation coefficient values, which is due to the fact that the elastic foundation coefficient of the conical shell gets harder in material terms and is added to its stability by increasing the values.

5 CONCLUSIONS

1. By increasing the amount of porosity coefficient (e_0) in the conical shell, the amount of critical buckling force decreases and the amount of critical buckling temperature increases.
2. The critical buckling temperature values in the second type distribution are less than the first type distribution.
3. As the angle of the apex of the cone in the conical shell increases, the critical buckling temperature decreases.
4. By increasing the value of R_a/h the critical buckling temperature of the conical shell decreases.
5. By increasing the values of L/R_a , the critical temperature values of the buckling of the conical shell decrease.

REFERENCES

[1] Eslami M.R., Ziaii A.R., Ghorbanpour A., 1996, Thermoelastic buckling of thin cylindrical shells based on improved donnell equations, *Journal of Thermal Stresses* **19**: 299-316.

[2] Najafizadeh M.M., Hasani A., Khazaeinejad P., 2009, Mechanical stability of functionally graded stiffened cylindrical shells, *Applied Mathematical Modelling* **33**: 1151-1157.

[3] Tornabene F., Viola E., Inman D.J., 2009, 2-D differential quadrature solution for vibration analysis of functionally graded conical, cylindrical shell and annular plate structures, *Journal of Sound and Vibration* **328**: 259-290.
[4] Tornabene F., 2009, Free vibration analysis of functionally graded conical, cylindrical shell and annular plate structures with a four-parameter power-law distribution, *Computer Methods* in *Applied Mechanics* and *Engineering* **198**: 2911-2935.
[5] Bagherizadeh E., Kiani Y., Eslami M.R., 2011, Mechanical buckling of functionally graded material cylindrical shells surrounded by Pasternak elastic foundation, *Composite Structures* **93**: 3063-7301.
[6] Bagherizadeh E., Kiani Y., Eslami M.R., 2012, Thermal buckling of functionally graded material cylindrical shells on elastic foundation, *AIAA Journal* **50**: 500-503.
[7] Sofiyev A.H., Kuruoglu N., 2013, Torsional vibration and buckling of the cylindrical shell with functionally graded coatings surrounded by an elastic medium, *Composites Part B* **45**: 1133-1142.
[8] Dung D.V., Hoa L.K., 2013, Nonlinear buckling and post buckling analysis of eccentrically stiffened functionally graded circular cylindrical shells under external pressure, *Thin-Walled Structures* **63**: 117-124.
[9] Dung D.V., Hoa L.K., 2013, Research on nonlinear torsional buckling and post-buckling of eccentrically stiffened functionally graded thin circular cylindrical shells, *Composites Part B* **51**: 300-309.
[10] Dung D.V., Hoa L.K., 2015, Semi-analytical approach for analyzing the nonlinear dynamic torsional buckling of stiffened functionally graded material circular cylindrical shells surrounded by an elastic medium, *Applied Mathematical Modelling* **39**: 6951-6967.
[11] Sabzikar Boroujerdy M., Naj R., Kiani Y., 2014, Buckling of heated temperature dependent FGM cylindrical shell surrounded by elastic medium, *Theoretical and Applied Mechanics* **52**(4): 869-881.
[12] Castro S., Mittelstedt C., Monteiro F., Arbelo M., Ziegmann G., Degenhardt R., 2014, Linear buckling predictions of unstiffened laminated composite cylinders and cones under various loading and boundary conditions using semi-analytical models, *Composite Structures* **118**: 303-315.
[13] Dung D.V., Nam V.H., 2014, Nonlinear dynamic analysis of eccentrically stiffened functionally graded circular cylindrical thin shells under external pressure and surrounded by an elastic medium, *European Journal of Mechanics - A/Solids* **46**: 42-53.
[14] Dung D.V., Hoa L.K., 2015, Research on nonlinear torsional buckling and post-buckling of eccentrically stiffened FGM cylindrical shell in thermal environment, *Composites Part B* **69**: 378-388.
[15] Asadi H., Kiani Y., Aghdam M.M., Shakeri M., 2016, Enhanced thermal buckling of laminated composite cylindrical shells with shape memory alloy, *Applied Composite Materials* **50**: 243-256.
[16] Tung H.V., 2014, Nonlinear thermomechanical stability of shear deformable FGM shallow spherical shells resting on elastic foundations with temperature dependent properties, *Composite Structures* **114**: 107-116.
[17] Tornabene F., Viola E., 2013, Static analysis of functionally graded doubly curved shells and panels of revolution, *Meccanica* **48**: 901-930.
[18] Bich D.H., Dung D.V., Nam V.H., 2013, Nonlinear dynamic analysis of eccentrically stiffened imperfect functionally graded doubly curved thin shallow shells, *Composite Structures* **96**: 384-395.
[19] Tornabene F., Fantuzzi N., Viola E., Reddy J.N., 2014, Winkler-Pasternak foundation effect on the static and dynamic analyses of laminated doubly curved and degenerate shells and panels, *Composites Part B* **57**: 269-296.
[20] Tornabene F., Fantuzzi N., Viola E., Batra R.C., 2015, Stress and strain recovery for functionally graded free-form and doubly curved sandwich shells using higher-order equivalent single layer theory, *Composite Structures* **119**: 67-89.
[21] Tornabene F., Fantuzzi N., Bacciocchi M., Viola E., Reddy J.N., 2017, A numerical investigation on the natural frequencies of FGM sandwich shells with variable thickness by the local generalized differential quadrature method, *Applied Sciences* **7**(131): 1-39.
[22] Tornabene F., Viola E., 2009, Free vibrations of four-parameter functionally graded parabolic panels and shells of revolution, *European Journal of Mechanics - A/Solids* **28**: 991-1013.
[23] Tornabene F.,Viola E., 2009, Free vibration analysis of functionally graded panels and shells of revolution, *Meccanica* **44**: 255-281.
[24] Mecitoglu Z., 1996, Vibration characteristics of a stiffened conical shell, *Journal of Sound and Vibration* **197**(2): 191-206.
[25] Rao S.S., Reddy E.S., 1981, Optimum design of stiffened conical shells with natural frequency constraints, *Composite Structures* **14**(1-2): 103-110.
[26] Sofiyev A.H., 2007, Thermoelastic stability of functionally graded truncated conical shells, *Composite Structures* **77**: 56-65.
[27] Sofiyev A.H., 2010, The buckling of FGM truncated conical shells subjected to combined axial tension and hydrostatic pressure, *Composite Structures* **92**: 488-498.
[28] Sofiyev A.H., 2015, Buckling analysis of freely supported functionally graded truncated conical shells under external pressures, *Composite Structures* **132**: 746-758.
[29] Sofiyev A.H., 2010, The buckling of FGM truncated conical shells subjected to axial compressive load and resting on Winkler- Pasternak foundations, *International Journal of Pressure Vessels and Piping* **87**: 753-761.
[30] Naj R., Boroujerdy M.S., Eslami M.R., 2008, Thermal and mechanical instability of functionally graded truncated conical shells, *Thin-Walled Structures* **46**: 65-78.

[31] Bich D.H., Phuong N.T., Tung H.V., 2012, Buckling of functionally graded conical panels under mechanical loads, *Composite Structures* **94**: 1379-1384.
[32] Torabi J., Kiani Y., Eslami M.R., 2013, Linear thermal buckling analysis of truncated hybrid FGM conical shells, *Composites Part B* **50**: 265-272.
[33] Sofiyev A.H., Kuruoglu N., 2013, Nonlinear buckling of an FGM truncated conical shells surrounded by an elastic medium, *International Journal of Pressure Vessels and Piping* **107**: 38-49.
[34] Dung D.V., Hoa L.K., Nga N.T., Anh L.T.N., 2013, Instability of eccentrically stiffened functionally graded truncated conical shells under mechanical loads, *Composite Structures* **106**: 104-113.
[35] Bahadori R., Najafizadeh M.M., 2015, Free vibration analysis of two-dimensional functionally graded axisymmetric cylindrical shell on Winkler–Pasternak elastic foundation by first-order shear deformation theory and using Navier-differential quadrature solution methods, *Applied Mathematical Modelling* **39**(16): 4877-4894.